# Evolution of mechanisms controlling epithelial morphogenesis across animals: new insights from dissociation - reaggregation experiments in the sponge Oscarella lobularis

**Amélie Vernale**
IMBE: Institut mediterraneen de biodiversite et d'ecologie marine et continentale
**Maria Mandela Prünster**
IBDML: Institut de Biologie du Developpement de Marseille
**Fabio Marchianò**
IBDML: Institut de Biologie du Developpement de Marseille
**Henry Debost**
IBDML: Institut de Biologie du Developpement de Marseille
**Nicolas Brouilly**
IBDML: Institut de Biologie du Developpement de Marseille
**Caroline Rocher**
IMBE: Institut mediterraneen de biodiversite et d'ecologie marine et continentale
**Dominique Massey-Harroche**
IBDML: Institut de Biologie du Developpement de Marseille
**Emmanuelle Renard**
IMBE: Institut mediterraneen de biodiversite et d'ecologie marine et continentale
**André Le Bivic**
IBDML: Institut de Biologie du Developpement de Marseille
**Bianca H. Habermann**
IBDML: Institut de Biologie du Developpement de Marseille
**Carole Borchiellini** (carole.borchiellini@imbe.fr)
IMBE: Institut mediterraneen de biodiversite et d'ecologie marine et continentale
https://orcid.org/0000-0003-0512-7724

**Research article**

**Keywords:** adherens junction, basement membrane, evolution, cytoskeleton remodeling, transcriptome, Porifera

**Posted Date:** April 1st, 2021

**DOI:** https://doi.org/10.21203/rs.3.rs-376467/v1



**Version of Record:** A version of this preprint was published at BMC Ecology and Evolution on August 21st, 2021. See the published version at https://doi.org/10.1186/s12862-021-01866-x.

# Abstract

Background: The ancestral presence of epithelia in Metazoa is no longer debated. Even though Porifera seem to be the best candidates to be the sister group to all other Metazoa, hardly anything is known about the proteins involved in the composition of cell-cell junctions or about the mechanisms that regulate epithelial morphogenetic processes in this phylum.

Results: To get insights into the early evolution of epithelial morphogenesis, we focused on morphogenic characteristics of the homoscleromorph sponge Oscarella lobularis. Homoscleromorpha are a sponge class with a typical basement membrane and adherens-like junctions unknown in other sponge classes. We took advantage of the dynamic context provided by cell dissociation-reaggregation experiments to explore morphogenetic processes in epithelial cells in an early lineage by combining fluorescent and electronic microscopy observations and RNA sequencing approaches at key time-points of the dissociation and reaggregation processes.

Conclusions: Our results show that part of the molecular toolkit involved in the loss and restoration of epithelial features such as cell-cell and cell-matrix adhesion is conserved between Homoscleromorpha and Bilateria, suggesting their common role in the last common ancestor of animals. In addition, Sponge-specific genes are differently expressed during the dissociation and reaggregation processes, calling for future functional characterization of these genes.


# Full Text

Due to technical limitations, full-text HTML conversion of this manuscript could not be completed. However, the manuscript can be downloaded and accessed as a PDF.

# Figures

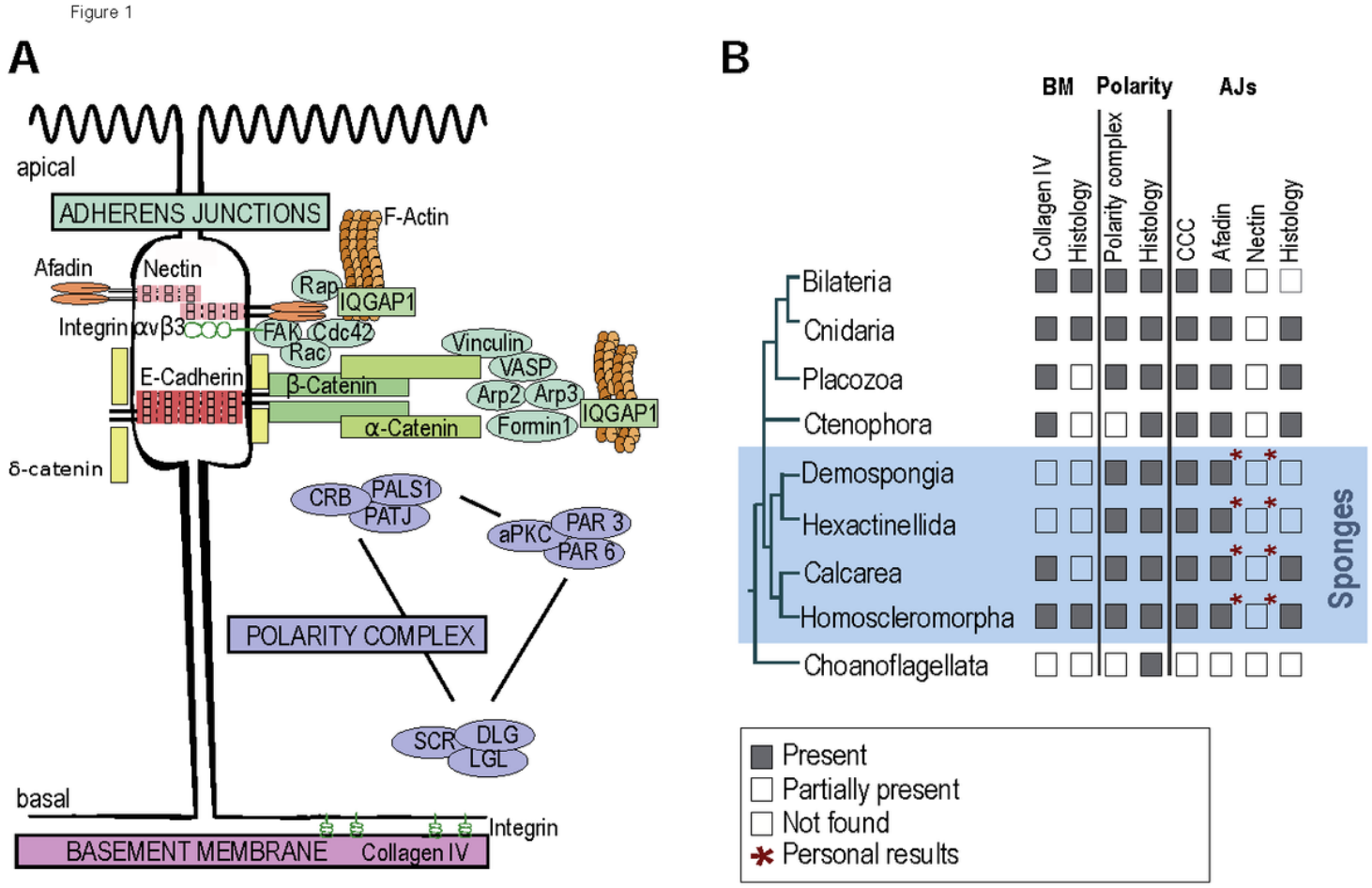


## Figure 1

The main molecular actors of epithelial cell features in bilaterians and their presence/absence in non-bilaterian metazoans. (A) Schematic representation (modified from (Miyoshi and Takai, 2011) of typical bilaterian epithelial cells and of proteins involved in (i) adherens junctions, (ii) the three polarity complexes and (iii) the basement membrane (Review in Renard et al., in press). (i) In detail, cell adhesion can be Nectin- and E-cadherin-based and connect via numerous proteins to the actin cytoskeleton: Nectins via Afadin and Integrin; E-adherins via δ-, β- and α-catenins to the cell adhesion complex proteins Vinculin, VASP, Formin, Arp2/3. In addition, Rap, Rac, CDC42, FAK and IqGAP1 regulate the changes and organization of the actin skeleton (Miyoshi and Takai, 2011). (ii) The three major polarity complexes namely the apically located PAR3/PAR6/aPKC complex and the CRUMBS (CRB)/PALS1/PATJ complex and along with a lateral SCRIBBLE (SCR)/DLG/LGL complex (Assémat et al., 2008). iii) The basement membrane of bilaterians involves mainly type IV collagen, laminins, perlecan and nidogen; laminins interact with integrins to establish cell-matrix adhesion (Fidler et al., 2017). The nomenclature chosen in the scheme is according to human proteins. (B) Presence/absence of epithelial histological features and epithelial genes in non-bilaterians mapped on a schematic representation of consensual phylogenetic relationships among metazoans according to the literature (for review see Kapli and Telford, 2020; Schenkelaars et al., 2019; Renard et al., in press). “Partially present” means that either only part of the genes were found in the considered taxa or that some species of the taxa lack the genes or features.

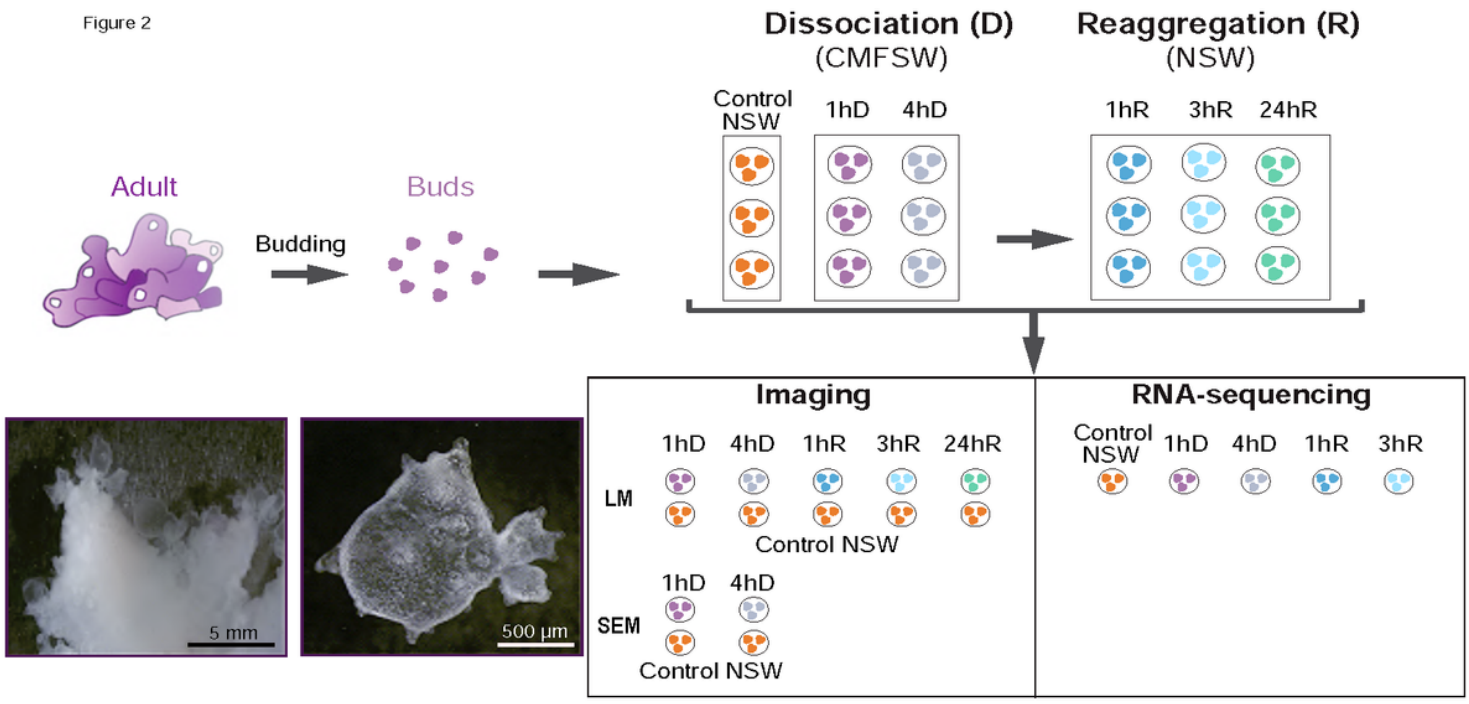


## Figure 2

Experimental strategy for the time course study of cell-dissociation and reaggregation processes in the homoscleromorph sponge Oscarella lobularis. Adults of Oscarella lobularis can reproduce asexually by budding, forming so-called buds. The bud tissues are highly similar to the adult tissues and buds were shown to be more convenient for experiments (Ereskovsky and Tokina, 2007; Rocher et al., 2020). Clonal buds from one adult were put in Calcium-Magnesium-Free Sea Water (CMFSW) to initiate cell dissociation. After 4 hours of dissociation buds were placed back into Natural Sea Water (NSW) to initiate reaggregation. Samples were collected at different times for imaging (Scanning Electron Microscopy (SEM), Light confocal Microscopy (LM)) and RNA-sequencing. Abbreviated as follows: 1hour (1hD) and 4hours (4hD) of dissociation and 1hour (1hR), 3 hours (3hR) and 24 hours (24hR) of reaggregation.

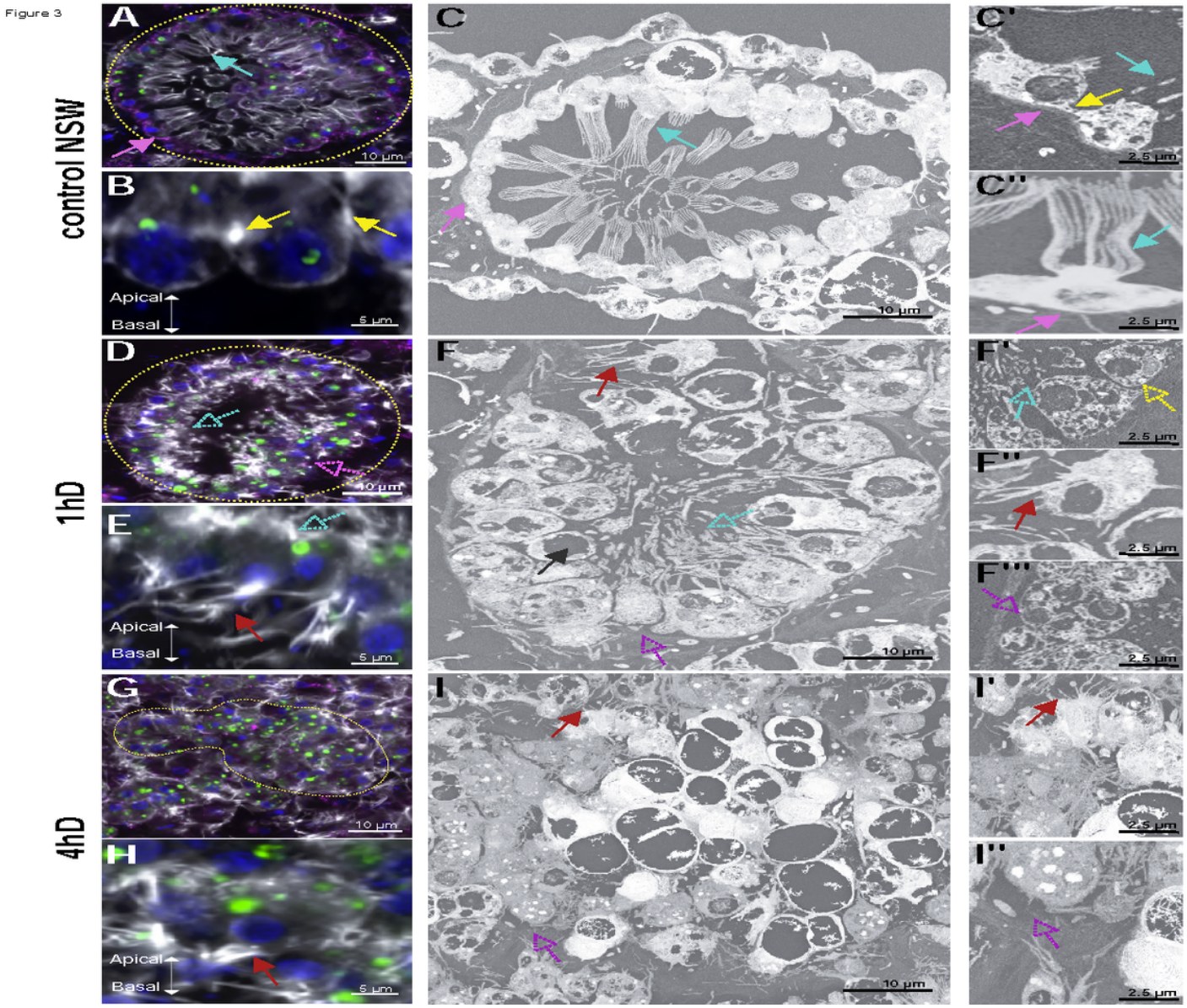


## Figure 3

Structural changes in the choanoderm during dissociation. (A- C”) Control conditions in natural sea water (1h NSW): (A) Confocal microscopic view (LM) of a choanocyte chamber, the classical round shape of the choanocyte chamber is visible (dotted yellow line) with its typical collar of apical microvilli (blue arrow). The type IV Collagen staining (in magenta) is lining the basal pole of choanocyte chambers (pink arrow). (B) LM focused view on the actin-rich cellular junction between choanocytes (yellow arrow). (C) Scanning Electron Microscopic (SEM) view of a choanocyte chamber with collar of apical microvilli (cyan arrow), and a basement membrane lining the choanocyte chamber (pink arrow). (C’) Focus on the cell-cell junction (yellow arrow), basal lamina (pink arrow) and apical microvilli (cyan arrow). (C”) Choanocyte with its complete apical microvilli collar (cyan arrow) and complete basal lamina (pink arrow). (D-F”’) Choanocyte chambers observed one hour after incubation in calcium-magnesium-free sea water (1hD CMSFW): (D) The general architecture of the choanocyte chamber is still observable in LM (dotted yellow line), immunostaining of type IV Collagen is not visible anymore (dotted pink arrow), apical microvilli are

disintegrated (dotted cyan arrow). (E) Focus (LM) on a choanocyte with its disintegrated apical microvilli (dotted cyan arrow) and numerous basal actin protrusions (red arrow). (F) SEM view of a choanocyte chamber. Choanocytes present vacuoles (black arrow), disintegrated apical microvilli (dotted cyan arrow) and protrusions (red arrow). The basal lamina is detached from the choanocytes (dotted pink arrow). (F') Focus (SEM) on the disintegration of the apical microvilli (cyan dotted arrow) and on the loss of cell-cell contact (dotted yellow arrow). (F") Focus on basal actin protrusions at the basal pole of a choanocyte (SEM) (red arrow). (F"') Focus on two choanocytes with a clear detachment from the basal lamina (dotted pink arrow). (G-I") Choanocyte chambers observed four hours after incubation in calcium-magnesium-free sea water (4hD CMFSW): (G) LM view of a destructured choanocyte chamber, immunostaining of type IV Collagen is not visible and the general architecture of the choanocyte chamber is no more recognizable (yellow dotted line). (H) (LM) Focus on a choanocyte with numerous actin basal protrusions (red arrow). (I) SEM view of choanocyte showing actin protrusions (red arrow) and the whole destructuring of the basal lamina (dotted pink arrow). (I') (SEM) focus on the actin protrusions (red arrow). (I") The basal lamina is completely lost at this time-point (SEM) (dotted pink arrow). For all confocal (LM) pictures: Staining in grey: Phalloidin, Green: PhaE lectin, Blue: DAPI, Magenta: type IV Collagen. Additional picture of control condition in NSW is available in the Supplementary Figure S2B.

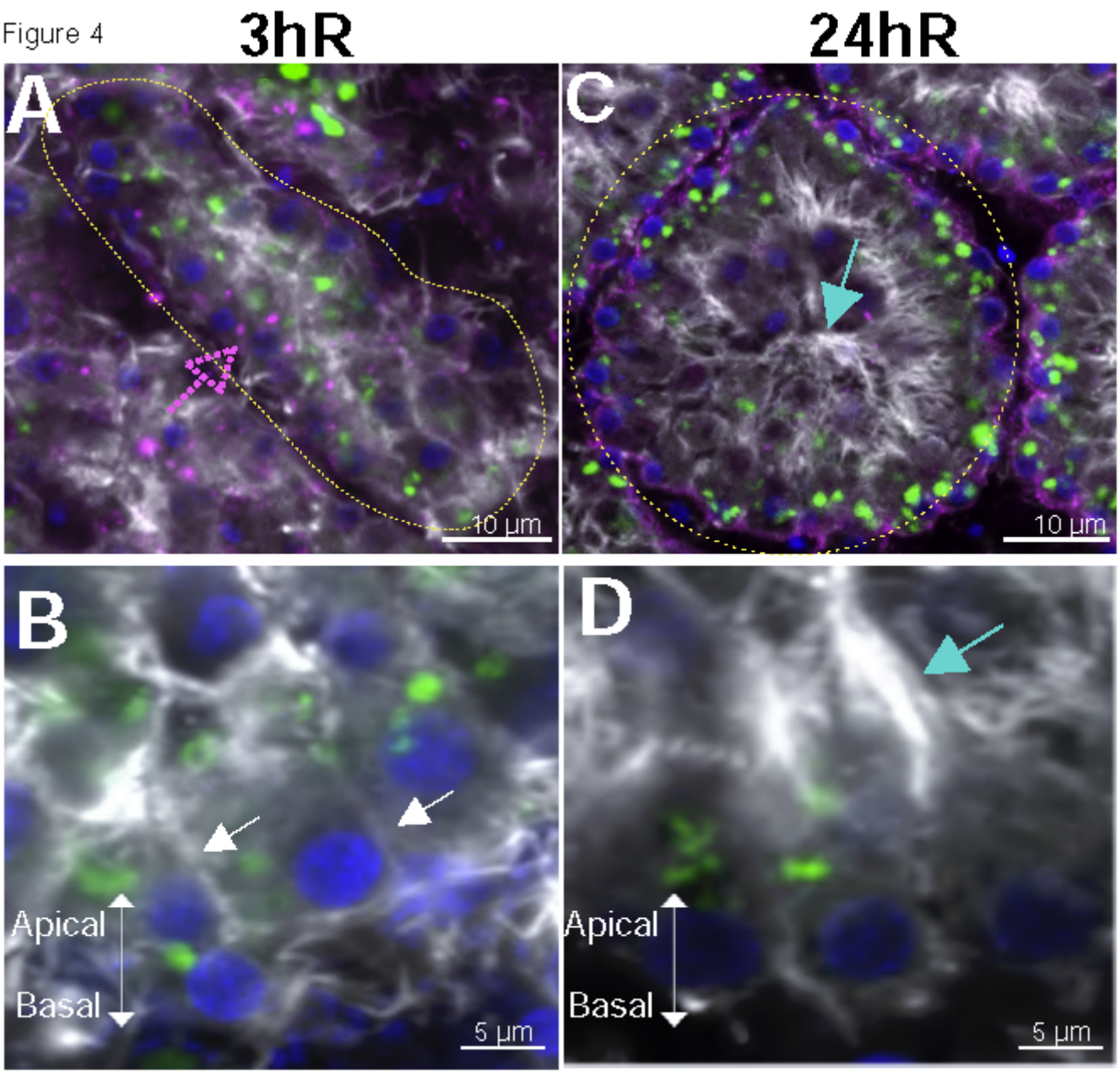


**Figure 4**

Restoration of the choanoderm during reaggregation. Confocal microscopic views of (A) a choanocyte chamber after 3 hours of reaggregation (3hR) in natural sea water (NSW), the immunostaining of type IV Collagen (in magenta) is discontinuous (dotted pink arrow). (B) Focus on three choanocytes starting to realign with each other at 3hR (white arrows). (C) A choanocyte chamber fully restructured after 24 hours of reaggregation (24hR), choanocytes present typical apical microvilli (cyan arrow). (D) Focus on choanocytes with a restored apical microvilli (cyan arrow). For all pictures, staining in grey: Phalloidin, in Green: Pha-E lectin, in Blue: DAPI, in Magenta: type IV Collagen. Additional views of control conditions in NSW are available in Supplementary Figures S2B.

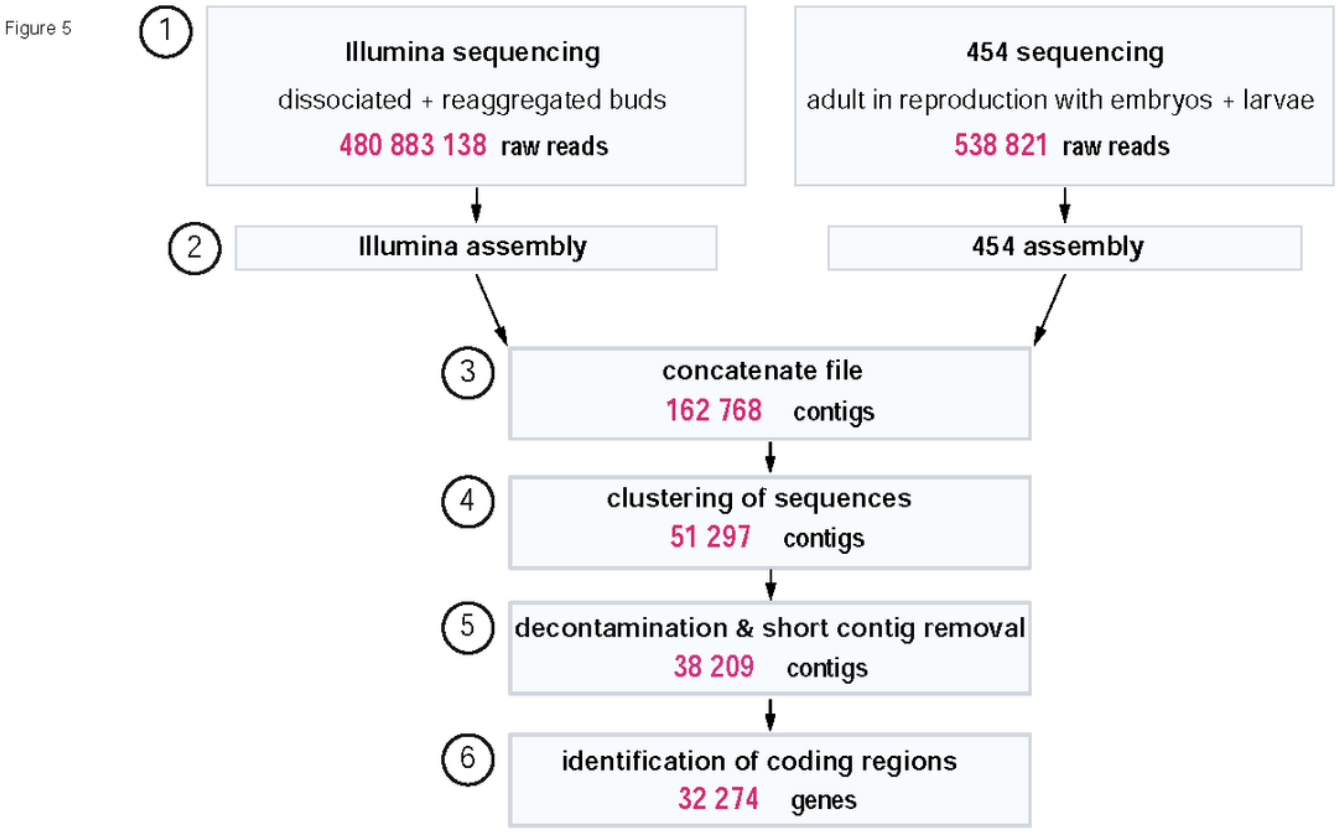


## Figure 5

Schematic workflow of the steps performed for de novo transcriptome assembly of Oscarella lobularis. (1) Illumina sequencing was performed on biological samples of 40 pooled clonal stage 3 buds exposed to the same conditions: dissociated in CMFSW and reaggregated in NSW. 454 sequencing was performed on tissue from one adult undergoing sexual reproduction containing a mixed population of embryos and pre-larvae collected in the bay of Marseille (Schenkelaars et al., 2015). Illumina reads were quality controlled using FastQC (http://www.bioinformatics.babraham.ac.uk/projects/fastqc/). Low-quality reads and adapters were removed using TrimGalore (https://github.com/FelixKrueger/TrimGalore). Illumina and 454 sequencing libraries were first de novo assembled individually and then merged. Illumina sequences were de novo assembled using Trinity. 454 reads were de novo assembled with Staden and GAP4 (Bonfield et al., 1995) by Eurofins. (2) The two assemblies were then concatenated. (3) Redundancy was reduced by clustering contigs > 80% identity with CD-hit EST (Li and Godzik, 2006) retaining the longer contig. (4) To remove sequence redundancy further, we indexed and mapped the contigs with GMAP (Wu and Watanabe, 2005) with a 95% sequence identity. To remove contaminants, we used Vecscreen and BlastN. (5) Using Transdecoder (https://github.com/TransDecoder) with the Transdecoder.predict option we were able to identify the most likely protein sequences encoded in open reading frames (ORFs) ≥ 100 aa. For additional experimental details see the Material and Methods section.

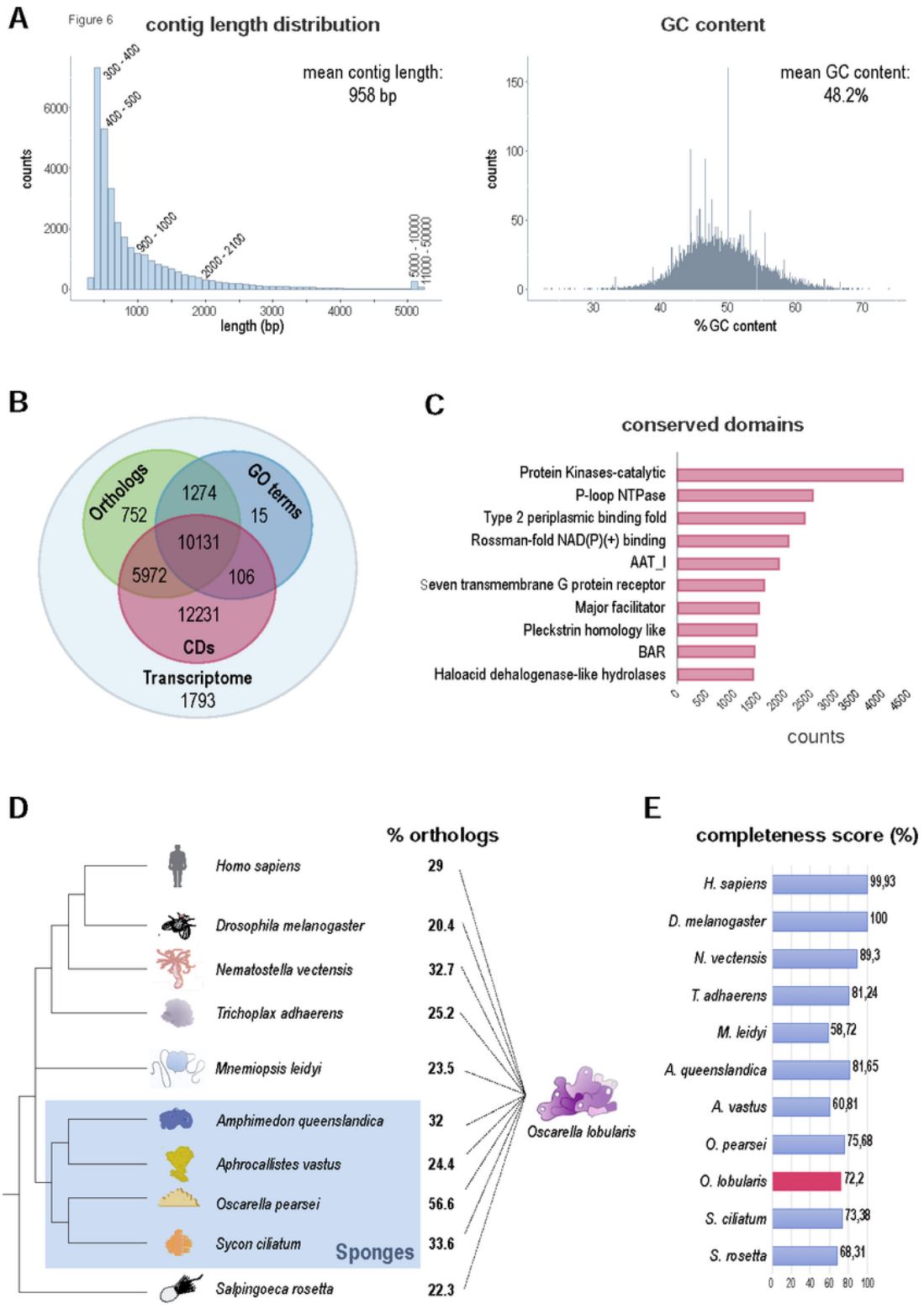


## Figure 6

Characteristics of the de novo transcriptome assembly of O. lobularis. (A) Contig length distribution and GC content of the O. lobularis transcriptome from mixed stages and types of sequencing. Statistics was done after de novo assembly, concatenation, decontamination, and length cleaning steps. The smallest contig is 255 bp long and the longest contig has 47 628 bp coming from a single long ORF encoding a Mucin ortholog. The average contig length is 958 bp. The mean percentage of GC content is 48.2 %. (B)

Annotated coding regions either with eggNOG (Huerta-Cepas et al., 2019) (orthologs) (18129 sequences), GO Terms (11526), and Conserved Domains (CDs) (Marchler-Bauer et al., 2011) (28440 sequences) (Supplementary Table S2). For 1793 contigs no described CD or ortholog could be found, corresponding to 5.5 % of the identified coding regions. (C) The ten most frequent Conserved Domains (CDs) in the O. lobularis transcriptome. Among the top ten CDs are kinases, nucleotide binding domains, domains that are involved in membrane transport or membrane binding as well as those inferring changes in cell shape. The protein kinase domain was most abundant and was present in 4057 coding regions. Occurrences were counted once per coding region. (D) Percentage of orthologs, O. lobularis has in common with other species. 29% orthologs are shared with human, 25.2% with Trichoplax adhaerens. Shared orthologs with other sponges vary from 24% to 57%. 56.6% of contigs from O. lobularis have a clear ortholog in its close relative, O. pearsei (Supplementary Table S3). (E) DOGMA analysis (Dohmen et al., 2016) to evaluate the completeness of different metazoan transcriptomes (Supplementary Table S5). For O. lobularis, we found 72.2% of expected CD arrangements. This is within the range of other sponge transcriptomes.

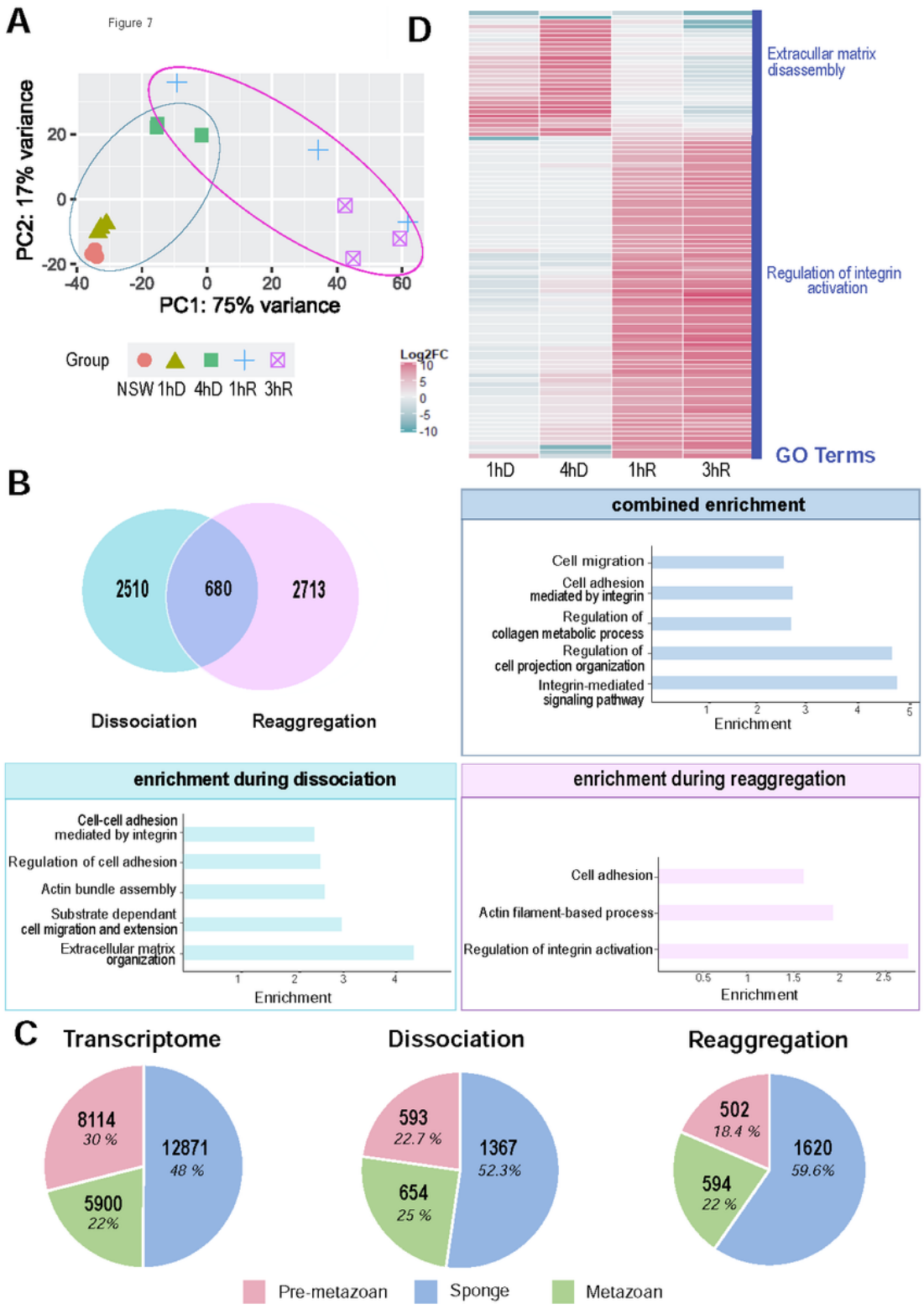


## Figure 7

Gene expression changes in O. lobularis buds during dissociation and reaggregation. (A) Principal component analysis (PCA) plot of the 5 different conditions sequenced during dissociation and reaggregation. Dissociation time-points are circled in blue, those of reaggregation in pink. Replicates cluster well except for the samples of the first hour of reaggregation (1hR) which show larger dispersion, and which are located between time-points of four hours of dissociation (4hD) and three hours of

reaggregation (3hR), indicating different reaggregation states of the sequenced buds. (B) A total of 5903 differentially expressed genes (DEGs) were found during dissociation and reaggregation with a log2 fold change (log2|FC|) of at least 1.5 (Supplementary Table S6). Pairwise comparisons were done as follows: for dissociation (1hD/CT, 4hD/CT); for reaggregation (1hR/4hD, 3hR/4hD); genes in common for both processes are shown as overlapping (680 genes). Gene ontology enrichment analysis of genes differentially expressed during dissociation shows that genes relevant for the process under study are enriched, including those involved in cell adhesion and its regulation, substrate dependent cell migration and actin bundle assembly were enriched (Supplementary Table S8). Enriched GO terms for shared DEGs of both conditions included cell migration, cell adhesion, regulation of collagen metabolic processes as well as integrin-mediated signaling pathway. During reaggregation, relevant GO terms associated with cell adhesion, regulation of integrin and actin filament-based process were enriched. (C) Phylostratigraphy analyses on the whole transcriptome and during dissociation and reaggregation provide the evolutionary age of differentially regulated genes during the dissociation and reaggregation process, as well as in the entire transcriptome of mixed stages. On the entire transcriptome 16.6% (5389) of the genes are O. lobularis specific (see Supplementary Table S7). During dissociation and reaggregation, there is a higher percentage of Sponge-specific DEGs as compared to the entire transcriptome. The percentage of metazoan DEGs is higher during dissociation than during reaggregation. Analysis was done after (Sogabe and Hatleberg, 2019). Species used are listed in Supplementary Table S7A. (D) Heatmap showing the hundred most differentially regulated genes during dissociation and reaggregation (1hD/CT, 4hD/CT, 1hR/4hD, 3hR/4hD). For genes upregulated during dissociation or reaggregation, we performed enrichment analysis for GO terms (with TopGO (Alexa, 2020)) (Supplementary Table S8B). Among the top enriched GO terms, we found regulation of extracellular matrix disassembly for dissociation and establishment and maintenance of an epithelium for the reaggregation.

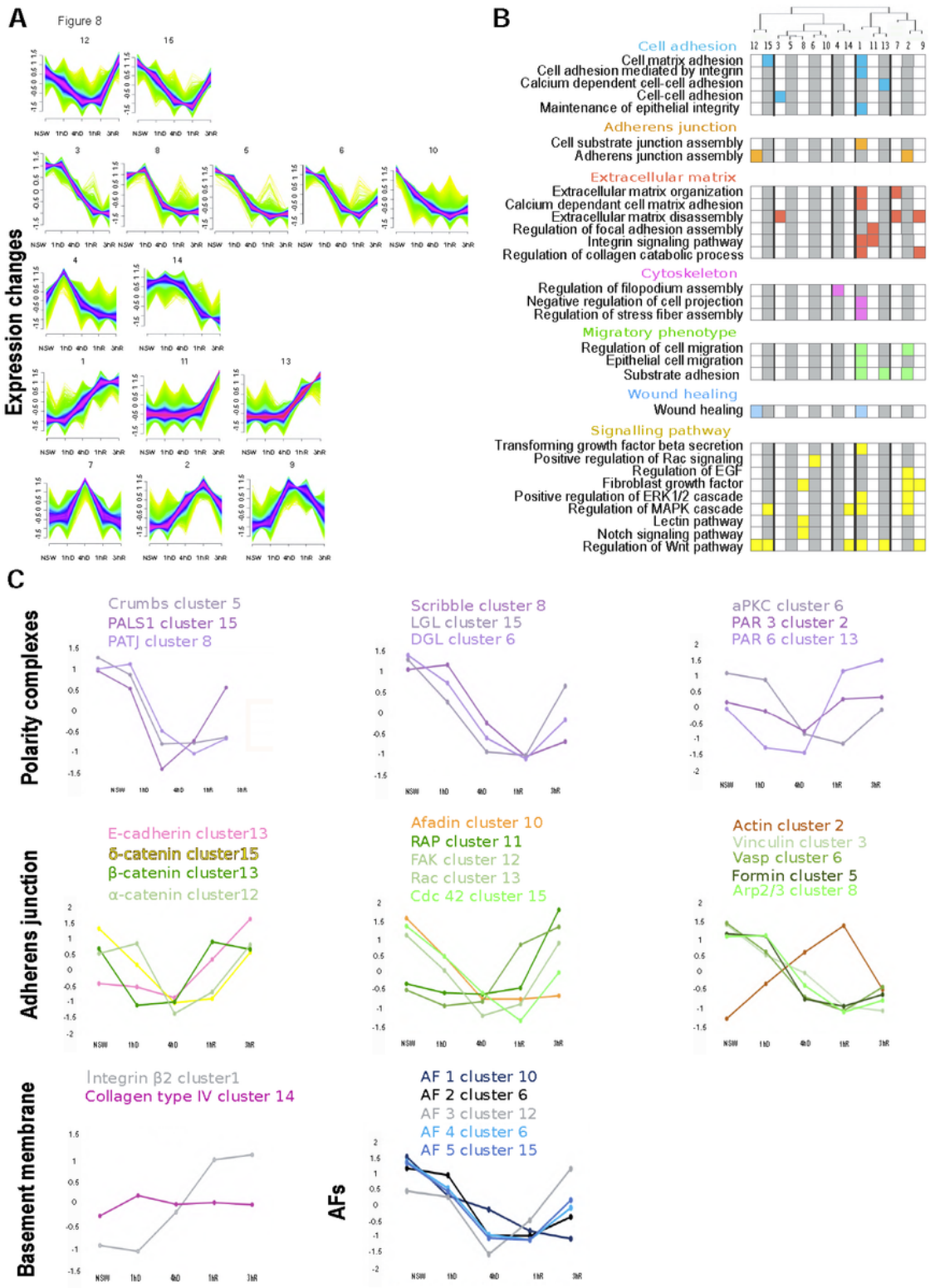


## Figure 8

Figure 8: Gene expression dynamics during dissociation and reaggregation. (A) Fuzzy clustering (Futschik and Carlisle, 2005) of temporal expression profiles during dissociation and reaggregation. We chose 15 clusters to represent our data, determined by hierarchical clustering of normalized read counts of the five conditions using hclust in R (Supplementary Figure S7). We found subgroups of profiles with a decrease in expression until 4hR (clusters 12,15), early peaks and a flat curve during reaggregation

(clusters 3,8,5,6,10), peaks at 1hR (clusters 4,14), decreasing expression during dissociation and increasing expression in reaggregation (clusters 1,11,13), strong ascending trends (clusters 10,5) and a peak at 4hD (clusters 7, 2, 9). Cluster cores have a membership value > 0.7 (pink) (Supplementary Table S10). Other membership values are shown as follows: membership value between 0.5 and 0.7 (blue), membership value < 0.5 (green). (B) Selected GO terms corresponding to Biological Processes found to be enriched for each core cluster as determined by topGO (Alexa, 2020)(Supplementary Table S8C). Colored boxes indicate significant enrichment in a given term (adj p-avlue <0.05). The dendrogram at the top was calculated by hierarchical clustering using hclust with Euclidian distance of the normalized read counts of genes qualifying as cluster core (membership value >0.7). (C) Expression profile of genes involved in epithelia organization and cell adhesion in bilaterians (see also Figure 1A). Expression of genes of the three polarity complexes decrease during dissociation and increase upon reaggregation. The expression of the gene coding for the basement membrane collagen was rather stable during the process, while the expression of integrin β2 increased at 4hD and became stable at 1hR. Genes involved in adherens junctions globally show a decrease in expression during dissociation and an increase around 1hR. Expression of the cytoskeleton component actin increased upon dissociation and decreased when reaggregation started. Finally, four of the Aggregation Factors (AFs) candidates (AF 1, 3, 4, 5) were downregulated during dissociation and upregulated during reaggregation (in particular AF3). In contrast, AF2 was downregulated during the entire process. NSW stands for natural condition which is the control condition, 1hD and 4hD correspond to 1 hour and 4 hours of dissociation (in CMFSW) respectively, 1hR and 3hR stand for 1 hour and 3 hours or reaggregation (in NSW) respectively. See Supplementary Table S11 for Standardized TPM and log2 Fold Change values.

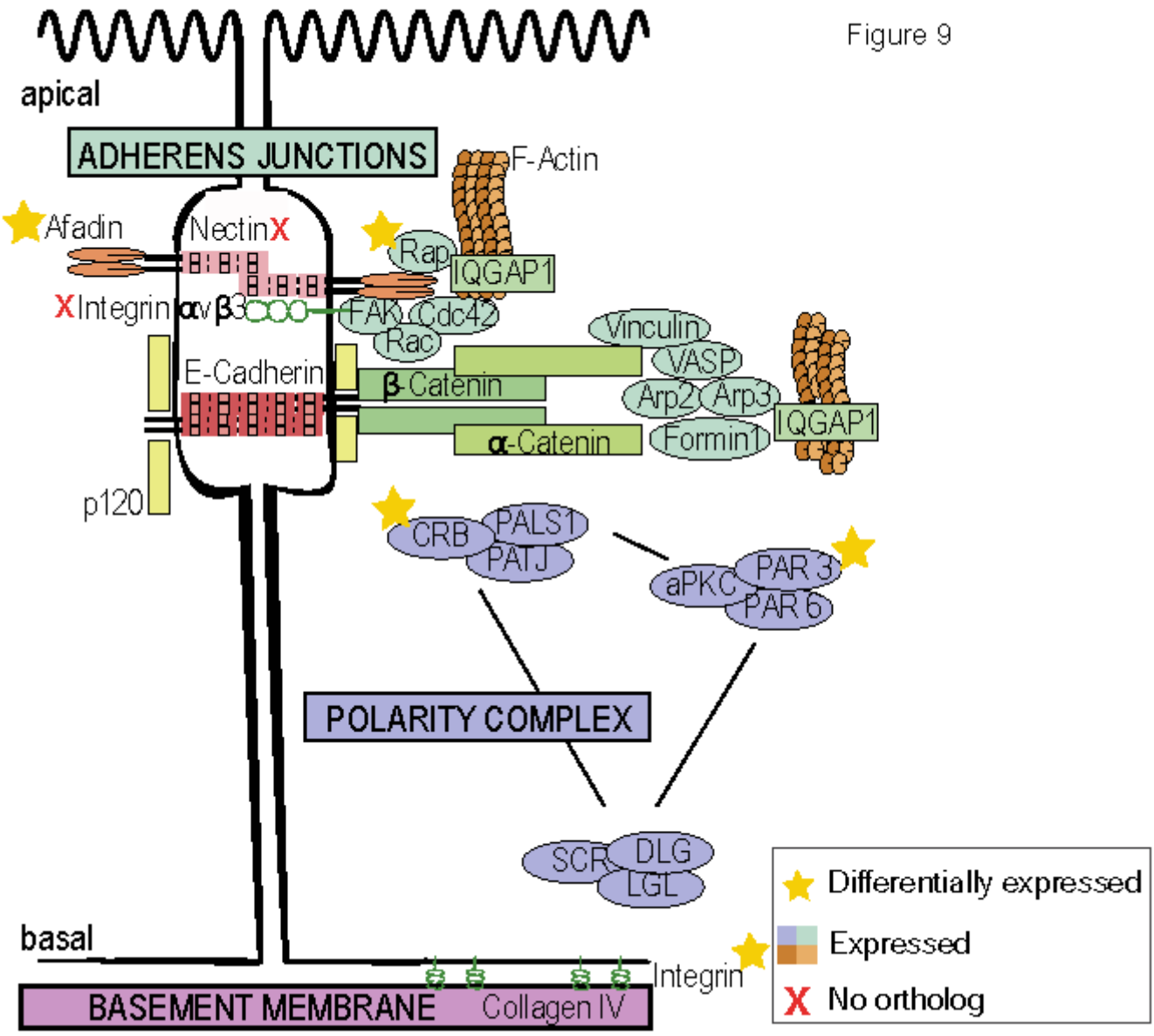


**Figure 9**

Gene expression of epithelial genes during the dissociation-reaggregation in Oscarella lobularis. Schematic representation of a bilaterian epithelial cell (Figure 1A) with the expression of the sponge genes coding for proteins involved in epithelial adhesion and maintenance during the dissociation-reaggregation experiment. For the genes involved in the adherens junctions, Afadin and Rap are differentially expressed at 4hD and 3hR, respectively. No orthologs were found for the Nectin and the Integrin αvβ3. In the polarity complex, Crumbs and Par3 are differentially expressed at 4hD. For the genes involved in the basement membrane, Integrin β2 is differentially expressed at 4hD. See Supplementary Table S11 for Standardized TPM and Log2FC values.

## Supplementary Files

This is a list of supplementary files associated with this preprint. Click to download.

- Supplementarymaterial.pdf